Interannual influences of the surface potential vorticity forcing over the Tibetan Plateau on East Asian summer rainfall

Chen SHENG[1, 2], Bian HE[*1, 2], Guoxiong WU[1, 2], Yimin LIU[1, 2], and Shaoyu ZHANG[1, 2]

[1]*State Key Laboratory of Numerical Modeling for Atmospheric Sciences and Geophysical Fluid Dynamics (LASG), Institute of Atmospheric Physics, Chinese Academy of Sciences, Beijing 100029, China*

[2]*College of Earth and Planetary Sciences, University of Chinese Academy of Sciences, Beijing 100049, China*

Submitted to *Advances in Atmospheric Sciences*

[*]Corresponding author: Bian HE

Email: heb@lasg.iap.ac.cn.

ABSTRACT

The influences of interannual surface potential vorticity forcing over the Tibetan Plateau (TP) on East Asian summer rainfall (EASR) and upper-level circulation are explored in this study. The results show that the interannual EASR and associated circulations are closely related to the surface potential vorticity negative uniform leading mode (PVNUM) over the TP. When the PVNUM is in the positive phase, more rainfall occurs in the Yangtze River valley, South Korea, Japan and part of northern China, less rainfall occurs in southeastern China, and vice versa. A possible mechanism by which PVNUM affects EASR is proposed. Unstable air induced by the positive phase of PVNUM could stimulate significant upward motion and lower-level anomalous cyclone over the TP. As a result, a dipole heating mode with anomalous cooling over the southwestern TP and anomalous heating over the southeastern TP is generated. Sensitivity experimental results regarding this dipole heating mode indicate that anomalous cooling over the southwestern TP leads to local and northeastern Asian negative height anomalies, while anomalous heating over the southeastern TP leads to local positive height anomalies. These results greatly resemble the realistic circulation pattern associated with EASR. Further analysis indicates that the anomalous water vapor transport associated with this anomalous circulation pattern is responsible for the anomalous EASR. Consequently, changes in surface potential vorticity forcing over the TP can induce changes in EASR.

Keywords: surface potential vorticity, East Asian summer monsoon, rainfall, the Tibetan Plateau

https://doi.org/ 10.1007/s00376-021-1218-4

Article Highlights:

- Potential vorticity (PV), inherently combining dynamics and thermodynamics, is an ideal indicator of the full forcing of the TP.
- The leading modes of EASR and upper-level circulation are closely related to the surface PV forcing over the TP.
- We highlight that the dipole heating mode over the TP plays a critical role in the process that TP's surface PV affects EASR.

1. Introduction

East Asian summer rainfall (EASR) affects East Asian countries, including China, Japan, and Korea (Ding and Chan, 2005; Kubota et al., 2016; Zhou et al. 2019). The changes and anomalies of EASR have caused frequent and severe weather disasters, including droughts, floods, and heatwaves (Huang et al., 2007; Huang et al., 2019). Many studies have investigated the possible driving factors of EASR. A basic consensus is that in addition to the El Niño-Southern Oscillation (ENSO) (Ding, 2007; Ding et al., 2020; Wang and Zhang, 2002; Wen et al., 2019; Xie et al., 2016), the Indian Ocean sea surface temperature anomaly (Xie et al., 2009; Yang et al., 2007), and the Indian summer monsoon rainfall (Kripalani and Kulkarni, 1997; 2001), the Tibetan Plateau (TP; e.g., Ye et al., 1957; Ye and Gao, 1979; Yanai et al., 1992; Liu et al., 2020) plays an important and nonnegligible role in EASR anomalies.

The TP, as the highest and broadest plateau on Earth, has increasingly attracted the attention of climatologists due to its large dynamic and thermodynamic effects on the climate of Asia. Previous studies demonstrated that the thermal forcing of the TP could greatly impact the Asian summer monsoon system (e.g., Ye et al., 1957; Flohn, 1957; Ye and Gao, 1979; Yanai et al., 1992; Wu et al., 1997, 2007, 2012, 2018; Xu et al., 2015). For example, Wu et al. (1997, 2007) indicated that sensible heating over the TP is the major driver of monsoon rainfall over the Asian continent. The strong surface sensible heating over the TP during boreal spring could affect the subsequent summer monsoon rainfall (Zhao and Chen, 2001; Duan et al., 2005). The onset, formation and evolution of the Asian summer monsoon are closely related to the thermal forcing of the TP (Wu and Zhang, 1998; Hsu and Liu, 2003). Moreover, some studies have examined the mechanical effects of the TP on the Asian summer monsoon system. Hahn and Manabe (1975) documented that the South Asian summer monsoon would not reach inland Asia if the TP is removed. More complex experiments with the uplift of the TP height from zero to its contemporary height (Chen et al., 1999; Liu, 1999; Kitoh, 2004; Jiang et al., 2008) indicated that the Asian summer monsoon rainfall spans northward from the Indian Ocean to inland Asia. Certain studies (Liu and Yin, 2002; Liang et al., 2005) illustrated that the onset and evolution of the Asian summer monsoon is also sensitive to the location and height of the TP. However, little insight is given about the intrinsic combined effects of dynamic and thermodynamic forcing of the TP in the literature.

Potential vorticity (PV; Rossby, 1940; Ertel, 1942), which inherently combines atmospheric dynamics and thermodynamics, is an ideal indicator to present the combined dynamic and thermodynamic conditions of the TP. Most previous studies have focused on atmospheric interior PV, where its impact on general circulation structure (e.g., Hoskins, 1991), rainstorms and cold air activities (e.g., Wu et al. 1995; Wu and Cai, 1997; Zhao and Ding, 2009) and its interannual relation to ozone (Danielsen 1968; Allaart et al. 1993; Folkins and Appenzeller, 1996; Sandhya et al. 2015) and Rossby wave breaking (Folkins and Appenzeller, 1996; Ryoo et al. 2013; Bowley et al., 2019) are the main interests. Instead of atmospheric interior PV, some studies (e.g., Hoskins, 1991) highlight the importance of surface PV based on the impermeability theorem (Haynes and McIntyre, 1987, 1999), especially the surface PV over the TP. For example, the elevated giant TP is a prominent surface PV source in the world (Sheng et al., 2021). In particular, the surface PV over the TP (TPPV) could exert a prominent influence on the TP vortex (Sheng et al., 2021), rainfall and extreme cold events downstream (Ma et al., 2019; Yu et al., 2019; Zhang et al., 2021). Although the surface PV is of great importance, the influence of surface TPPV forcing on EASR is still a knowledge gap.

The present paper aims to illustrate the interannual impact of the surface TPPV forcing associated with the intrinsic combined effect of the dynamics and thermodynamics of the TP on EASR. The remainder of the paper is organized as follows. Section 2 presents the data, method, and model. In section 3, the relationships of surface TPPV forcing with EASR and EASR-related circulation are presented. Section 4 analyzes the possible mechanism of how surface TPPV forcing affects EASR. Finally, conclusions and discussion are provided in section 5.

2. Data, method and model

2.1 Data

Monthly mean data on the hybrid σ–p model level obtained from MERRA2 (Rienecker et al., 2011; Lucchesi, 2012) are used to calculate the surface PV and surface static stability. Variables include the air temperature, zonal and meridional wind, and pressure.

Data used in this study also include monthly outgoing longwave radiation (OLR) from the polar-orbiting series of satellites of the National Oceanic and Atmospheric Administration (Liebmann and Smith 1996); monthly land precipitation data from the Climatic Research Unit (Mitchell and Jones, 2005); and monthly specific humidity, monthly zonal, meridional and vertical wind on the pressure level from MERRA2.

The study period is 1980-2017. The horizontal resolution of all MERRA2 data is 0.625° × 0.5° (longitude × latitude). The horizontal resolutions of the OLR and precipitation data are 2.5° × 2.5° and 0.5° × 0.5°, respectively. Climate mean values calculated over June, July, and August (JJA) are used to represent the boreal summer condition.

2.2 Method

Surface PV is calculated as follows (Sheng et al., 2021):

$$\begin{aligned} PV &= \alpha_h \vec{\xi}_{ah} \cdot \nabla_h \theta \\ &= g[\frac{\partial v}{\partial p}(\frac{\partial \theta}{\partial x})_h - \frac{\partial u}{\partial p}(\frac{\partial \theta}{\partial y})_h] \ - g[f + (\frac{\partial v}{\partial x})_h - (\frac{\partial u}{\partial y})_h]\frac{\partial \theta}{\partial p} , \end{aligned}$$

where g is gravity, which is 9.8 m/s^2; p is pressure; θ is potential temperature; f is the Coriolis parameter; (u, v) is horizontal wind; and h indicates that the horizontal difference is carried out at the hybrid σ–p level. The surface PV is obtained from the two bottom levels at the hybrid σ–p level. More details about the calculation of surface PV can be found in Sheng et al. (2021).

The surface static stability is calculated as $-\frac{\partial\theta}{\partial p}$, where θ and p are obtained from the two bottom levels at the hybrid σ–p level.

The horizontal water vapor flux (WVF) is calculated as follows:

$$WVF = \vec{V}q = (uq, vq),$$

where q is specific humidity.

Statistical methods, including linear regression, linear correlation, Student's t test, empirical orthogonal function (EOF), and multivariate EOF (MVEOF), are used in this study. The linear trends and decadal variation (more than nine years) in the data are removed to highlight the interannual variability.

2.3 Model

The linear baroclinic model (LBM) (Watanabe et al., 1999; Watanabe and Kimoto, 2000) is employed to investigate the responses of the upper-level circulation regarding the surface PV forcing over the TP. The model used in this study has 20 σ vertical levels. The horizontal level is represented by spherical harmonics with a resolution of T42. More details about the model description can be found in Watanabe and Jin (2003). The LBM is a time-varying model that linearizes the basic state based on primitive equations. We take boreal summer climatology as the basic state in this study. Since dissipation terms including biharmonic horizontal diffusion, weak vertical diffusion, Newtonian damping and Rayleigh friction are adopted, the model response reaches its steady state at approximately 14 days. Therefore, we use the results averaged from the last 15 days in the 30-day integration for analysis.

3. Results

3.1 Leading mode of surface TPPV, EASR, and upper-level circulation

EOF analysis is applied to analyze the dominant temporal and spatial features of the surface TPPV, EASR, and circulation over East Asia during boreal summer for the 1980-2017 period. Figure 1(a) shows the first leading mode of the EOF (EOF1) on the summer surface TPPV. The variation in surface PV on the southern slope and in the southeastern corner of the TP has the opposite sign to that in the main TP platform. Although the signs of the surface PV in the two areas are opposite, the southern area is quite small. In general, the distribution of EOF1 on surface PV shows a negative uniform mode (PVNUM). The corresponding normalized first principal component of the EOF pattern (PC1) is defined as the surface PV index (PVSI; red line), as shown in Figure 1(d). The variance percentage explained by the first leading mode is 36%.

Figure 1(b) shows the EOF1 of EASR. The corresponding normalized PC1 is defined as the precipitation index (PreI; blue dashed line), as shown in Figure 1(d). The maximum variation center of EASR occurs in the Yangtze River valley, South Korea, Japan (YKJ), and southern China. The variation in EASR in YKJ has the opposite sign to that in southern China. There is also a relatively weak dipole variation mode in northern China. The dominant mode of EASR obtained in this study is generally consistent with that obtained by Zuo et al. (2011).

Using the NCEP-NCAR reanalysis over mid-latitude Asia in JJAS (i.e., June, July, August, and September) from 1948 to 1998, Wu (2002) identified an interannual dominant pattern in the upper-level winds called the mid-latitude Asian summer (MAS) pattern. The MAS pattern in his study features two anomalous cyclones, with one centered at 37.5 °N, 65 °E and the other centered at 42.5 °N, 130 °E. Following Wu (2002), we applied MVEOF analysis to the 200 hPa wind anomaly to reveal the dominant circulation mode over mid-latitude Asia during boreal summer. The domain for the MVEOF analysis is 20-60 °N, 50-150 °E, and the result is not sensitive to the domain. The first leading mode of MVEOF (MVEOF1) is shown in Figure 1(c), and the corresponding normalized PC1 is defined as the mid-latitude Asian summer index (MASI; black dashed line) shown in Figure 1(d). Figure 1(c) shows that two anomalous cyclones are centered northwest of the TP and northeastern Asia. In between the two large cyclones is an anticyclone over the southeastern corner of the TP. The anticyclone identified in this study is more prominent than that in Wu (2002), which is partly because of the different reanalysis data and partly because of the different periods. From high to low latitudes, the positive MAS generally shows a "CCA" pattern (i.e., cyclone-cyclone-anticyclone pattern). Correspondingly, the negative MAS generally shows an "AAC" pattern (i.e., anticyclone-anticyclone-cyclone pattern).

To investigate the relationship of surface TPPV forcing with the EASR and upper-level circulation over East Asia, Figure 1(d) shows the time series of PVSI, MASI, and PreI. PVSI shows significant correlations with PreI and MASI, with yield correlation coefficients of 0.56 and 0.74 (both passing the 0.05 significance level), respectively. These results indicate that the EASR and the leading mode of circulation (i.e., MAS pattern) over East Asia are closely related to the surface TPPV forcing.

3.2 Relationship of surface TPPV forcing with EASR and associated circulation

Figure 2 shows the spatial pattern of the correlation coefficients between the PVSI and EASR anomalies. The pattern (Figure 2) is similar to EOF1 of EASR (Figure 1b). A negative correlation appears in southern China, whereas positive correlations are observed in YKJ. A positive correlation but with a small area appears in part of northern China. The correlation coefficients in these regions are significant at the 0.05 significance level. A weak negative correlation is seen in the area south of northern China (approximately 42 °N), but this correlation is not significant. These results indicate that the positive phase of PVNUM is associated with more rainfall in YJK, part of northern China and less rainfall in southern China, and the negative phase of PVNUM is related to the opposite rainfall pattern.

To understand the comprehensive three-dimensional relationship between surface TPPV forcing and EASR, the correlation patterns between the PVSI, PreI and circulation anomalies at different levels are shown in Figure 3. Figures 3a-c show correlation coefficients between PVSI and circulation at different levels. Corresponding to the positive (negative) PVNUM, at 200 hPa (Figure 3a), two anomalous cyclones (anticyclones) appear at middle latitudes at approximately 40°N. One center is located northwest of the TP, and the other is located in northeastern China (Figure 3a). In addition to these two anomalous cyclones (anticyclones), an anomalous anticyclone (cyclone) center appears at the southeastern corner of the TP. This configuration generally shows the MAS pattern (Figure 1b). Except for the anomalous cyclone (anticyclone) over the northwestern TP at 850 hPa (Figure 3c), this equivalent barotropic pattern can also be seen at the middle (Figure 3b) to lower (Figure 3c) levels. The correlation between PreI and circulation (Figures 3d-3f) closely resembles Figures 3a-c, which further confirms that surface TPPV forcing is significantly related to EASR. In addition, comparing Figures 3a-c and Figures 3d-f reveals that the MAS pattern plays an important role in the connection between surface TPPV forcing and EASR.

4. Possible mechanism of the surface TPPV forcing affecting the EASR

To investigate the possible mechanism of surface TPPV forcing affecting EASR, the LBM is employed in this section to examine the response of upper circulation regarding the anomalous heating related to surface TPPV forcing.

4.1 Diagnostic analysis

Surface PV is closely related to the static stability within the surface layer. Figure 4a shows the correlation coefficient between PVSI and static stability anomalies. The correlation between the PVSI and horizontal wind anomalies at surface and vertical motion (omega) anomalies at 500 hPa are shown in Figure 4b. Corresponding to the positive phase of PVNUM, the anomalous static stability over the whole TP is significantly negative (Figure 4a). This result means that the air within the surface layer over the TP is anomalously statically unstable. As a result, the anomalous omega is significantly negative, accompanied by anomalous upward motion occurring at the main body of the TP (Figure 4b). Consequently, a significant anomalous cyclonic circulation is generated south of the TP at the surface (Figure 4b). The negative phase of PVNUM corresponds to the opposite situation of surface static stability and circulation pattern.

The anomalous south and north winds associated with the anomalous circulation to the south of the TP (Figure 4b) induced by surface TPPV forcing could lead to anomalous heating over the TP. Figure 5 shows the correlation coefficient between

PVSI and OLR (Figure 5a) and regressed rainfall anomalies against PVSI (Figure 5b) to examine the distribution of anomalous heating. A dipole mode of the OLR anomalies is clearly observed in Figure 5a. Corresponding to the positive phase of PVNUM, positive OLR anomalies cover the southwestern TP to northern India. The highest negative OLR anomalies mainly occur on the eastern TP, whereas the highest positive OLR anomalies mainly occur on the western TP. The anomalous cyclonic circulation (Figure 4b), with cool and divergent flow to its western part and wet, warm flow to its eastern part, accounts for this clear dipole mode of the OLR (Figure 5a). Consistent with the OLR, the rainfall anomalies also show a dipole mode (Figure 5b) with less rainfall over the southwestern TP and northern India and more rainfall over the eastern TP. The rainfall anomalies indicate that the strongest negative and positive condensational heating anomalies occur at the southwestern TP to northern India and the eastern TP, respectively. Corresponding to the negative phase of PVNUM, the situation is on the opposite.

4.2 Sensitivity experiments

The response of upper-level circulation to the negative heating anomaly over northern India has been examined in Wei et al. (2014). Because the lower latitude of the negative heating anomaly over northern India (Figure 5b) is far away from the westerly jet (light green shading in Figure 7) at high latitudes in the north, the associated atmospheric response regarding the negative heating anomaly over northern India is trapped south of 40°N (Wei et al., 2014; see their Figure 8), exhibiting a zonal dipole mode with an anomalous cyclone to the west of 80°E and an anomalous anticyclone to the east of 80°E. There are some differences between the circulation caused by the negative heating anomaly over northern India (Wei et al., 2014; see their Figure 8) and the MAS pattern (Figure 3) related to EASR. Hence, regarding the negative heating anomalies centered on the southwestern TP and northern India, we focus on the southwestern TP in this study.

Based on the diagnostic analysis of heating anomalies induced by surface TPPV forcing, three groups of experiments are conducted. Exp1 is an experiment of positive heating over the southeastern TP (Exp1, Figures 6a-b). Exp2 is an experiment of negative heating over the southwestern TP (Exp2, Figures 6c-d). Exp3 is an experiment of combined positive and negative heating over the southeastern and southwestern TP, respectively (Exp3, Figure 6e). According to the reanalysis, the heating centers are at 30°N, 99°E and 75°N, 32°E in Exp1 and Exp2, respectively. The peak of the ideal heating profile in both the Exp1 and Exp2 experiments is 1.0 K/day and -1.0 K/day, respectively. The peaks in the heating profile are at $\sigma = 0.6$ and $\sigma = 0.4$ in Exp1 and Exp2, respectively. Since the LBM is a linear model, the heating configuration (Figure 6e) and atmospheric response (Figure 7c) in Exp3 are linear combinations of Exp1 and Exp2.

The atmospheric responses are shown in Figure 7. In Exp1 (Figure 7a), the positive heating anomaly over the eastern TP triggers a local anomalous anticyclone and high height at 200 hPa. The anomalous high is strengthened locally with slight northward and westward dispersion. In Exp2 (Figure 7b), the negative heating anomaly over the southwestern TP stimulates a local anomalous cyclone and low height at 200 hPa. Compared with Wei et al. (2014), because the location of the negative heating center over the southwestern TP is farther north than that over northern India, the anomalous cyclone could trigger waves in the westerly jet and lead to an anomalous cyclone downstream over northeastern China. In Exp3 (Figure 7c), the response of atmospheric circulation with "CCA" is very similar to the MAS pattern related to EASR (Figures 3d-f). These results indicate that the dipole heating mode induced by surface TPPV forcing can lead to a realistic MAS pattern, which is important for the formation of the anomalous EASR.

4.3 Influence of circulation anomalies on EASR

The above results indicate that surface TPPV forcing can lead to the formation of the MAS pattern. In this section, we examine how the MAS pattern affects the EASR anomalies.

Rainfall anomalies are related to water vapor transport anomalies and their divergence at the lower level. Since atmospheric moisture is mainly concentrated at the middle to lower level, Figure 8 shows the correlation between PVSI and WVF and its divergence at 500 hPa (Figure 8a) and 850 hPa (Figure 8b). Generally, the anomalous WVF (Figure 8) shows an equivalent barotropic structure. This equivalent barotropic structure markedly resembles the MAS pattern. Corresponding to the positive phase of PVNUM, the anomalous cyclonic WVF (Figure 8) over northeastern China embedded in the MAS pattern converges water vapor over South Korea and Japan and cooperating with the southern anticyclonic WVF, converges the wet, warm southwesterly flow and dry, cold northerly wind to the Yangtze River valley. In addition, an anomalous convergence of WVF (Figure 8) occurs in part of northern China. Hence, the EASR over YKJ and part of northern China is greater than normal (Figure 2). Although the WVF transfers water vapor to southern China, the WVF is divergent. Thus, the EASR over southern China is lower than normal (Figure 2). Corresponding to the negative phase of PVNUM, the situation is on the opposite. These results indicate that the WVF anomalies related to the MAS pattern are responsible for the EASR anomalies.

5. Conclusion and discussion

The present study investigates the relationship between the surface PV forcing over the TP and EASR and the associated circulation on the interannual timescale and the possible mechanism. The main conclusions obtained from the results are described as follows.

The correlation between the time series of the leading mode of the surface PV forcing over the TP (i.e., PVNUM) and EASR and the leading mode of upper-level circulation (i.e., MAS pattern) are as high as 0.56 and 0.74, respectively. Moreover, the circulation related to PVNUM greatly resembles the circulation associated with EASR. These results indicated that the interannual EASR and related upper-level circulation over East Asia are closely linked to the surface PV forcing over the TP, and the MAS pattern plays an important role in the PVNUM affecting EASR. Diagnostic analysis indicates that the positive phase of PVNUM could lead to unstable air within the surface layer over the TP. As a result, anomalous upward motion and cyclonic circulation are generated over the TP. Induced by cyclonic circulation, a dipole heating mode with anomalous cooling over the southwestern TP and anomalous heating over the southeastern TP appeared. Sensitivity experiments prove that the dipole heating mode associated with the surface PV forcing over the TP can trigger the MAS pattern related to EASR anomalies. The MAS pattern converges water vapor to the Yangtze River valley, South Korea, Japan and part of northern China and diverges water vapor over southern China. Therefore, the EASR over the Yangtze River valley, South Korea, Japan and part of northern China is greater than normal, and that over southern China is lower. The negative phase of PVNUM is related to the opposite rainfall and circulation pattern. Consequently, the surface PV forcing over the TP exerts a significant influence on EASR by changing the air static stability within the surface layer over the TP and causing the dipole heating mode and the subsequent anomalous water vapor transport related to the MAS pattern.

The aforementioned major mechanism is briefly shown schematically in Figure 9. In summary, PVNUM triggers lower-level cyclonic circulation by reducing the surface static stablity (Figure 9b). The dipole heaing mode induced by this cyclonic circulation could lead to anomalous circulation at the upper level (Figure 9a). As a result, the anomalous water vapor transport (Figure 8) embedded in the upper-level anomalous circulation is responsible for EASR anomalies (Figure 9c).

Previous studies (e.g., Wu, 2002) show that the MAS pattern is related to the Indian summer monsoon. We calculated the concurrent correlation coefficient between the MASI and Indian summer monsoon index (defined by Wang et al., 2001) and found that the correlation coefficient reaches -0.45, passing the 0.05 significance test; however, when the index of the surface TPPV forcing (i.e., PVSI, red line in Figure 1d) is removed, it is reduced to -0.28, which does not pass the significance test. This result further confirms the important role of surface TPPV forcing on EASR. ENSO is the most prominent interannual signal in climate systems. We also calculated the correlation between the summer PVSI and NINO3.4 index (SST averaged over the region 5°S-5°N, 120°-170°W; https://psl.noaa.gov/data/climateindices/list/) in the preceding winter and concurrent summer. The coefficients are 0.21 and -0.18, respectively, which do not pass the significance test, meaning that the relationship between surface TPPV forcing and EASR is unaffected by ENSO.

The present study only focuses on the impacts of TP on monsoon rainfall over East Asia. The complicated Asian summer monsoon system, greatly affected by the TP, includes the South Asian summer monsoon and the East Asian summer monsoon.

Research on the relationship between the PV anomaly over the TP and monsoon rainfall as well as wind fields over the Asian region will be conducted in the future. In this study, although the simple model (e.g., LBM) clearly shows the impact of surface TPPV forcing on EASR, it is still necessary to use the fully coupled model to examine the surface TPPV-rainfall-circulation feedback to understand the interactions between the surface TP forcing and EASM system. Furthermore, with the help of the PV budget equation, the relative importance of dynamic PV advection, PV generation due to diabatic heating, and friction effects to the variation of surface PV will be quantificationally answered, which will advance our understanding of the TP's impacts greatly.

Acknowledgments. We thank the reviewers for their constructive suggestions and comments. This work is jointly supported by the National Natural Science Foundation of China (91837101, 91937302, and 41730963) and the National Key Research and Development Program of China (Grant No. 2018YFC1505706).

REFERENCES

Allaart, M. A. F., H. Kelder, and L. C. Heijboer, 1993: On the Relation between Ozone and Potential Vorticity. *Geophysical Research Letters*, **20**, 811-814.

Bowley, K. A., J. R. Gyakum, and E. H. Atallah, 2019: A New Perspective toward Cataloging Northern Hemisphere Rossby Wave Breaking on the Dynamic Tropopause. *Monthly Weather Review*, **147**, 409-431.

Chen, L. X., J. P. Liu, X. J. Zhou, and P. X. Wang, 1999: Impact of Uplift of Qinghaixizang Plateau and Change of Land-Ocean Distribution on Climate over Asia. *Acta Meteorologica Sinica*, **4**, 314-329.

Danielsen, E. F., 1968: Stratospheric-Tropospheric Exchange Based on Radioactivity Ozone and Potential Vorticity. *Journal of the Atmospheric Sciences*, **25**, 502-518.

Ding, Y., 2007: The Variability of the Asian Summer Monsoon. *Journal of the Meteorological Society of Japan*, **85B**, 21-54.

Ding, Y. H., and J. C. L. Chan, 2005: The East Asian Summer Monsoon: An Overview. *Meteorology and Atmospheric Physics*, **89**, 117-142.

Ding, Y. H., P. Liang, Y. J. Liu, and Y. C. Zhang, 2020: Multiscale Variability of Meiyu and Its Prediction: A New Review. *Journal of Geophysical Research-Atmospheres*, **125**, 28.

Duan, A. M., Y. M. Liu, and G. X. Wu, 2005: Heating Status of the Tibetan Plateau from April to June and Rainfall and Atmospheric Circulation Anomaly over East Asia in Midsummer. *Science in China Series D-Earth Sciences*, **48**, 250-257.

Ertel, H., 1942: Ein Neuer Hydrodynamische Wirbelsatz. *Meteorologische Zeitschrift Braunschweig*, **59**, 33-49.

Flohn, H., 1957: Large-Scale Aspects of the &Ldquo;Summer Monsoon&Rdquo; in South and East Asia. *Journal of the Meteorological Society of Japan*, **35A**, 180-186.

Folkins, I., and C. Appenzeller, 1996: Ozone and Potential Vorticity at the Subtropical Tropopause Break. *Journal of Geophysical Research-Atmospheres*, **101**, 18787-18792.

Hahn, D. G., and S. Manabe, 1975: Role of Mountains in South Asian Monsoon Circulation. *Journal of the Atmospheric Sciences*, **32**, 1515-1541.

Haynes, P. H., and M. E. McIntyre, 1987: On the Evolution of Vorticity and Potential Vorticity in the Presence of Diabatic Heating and Frictional or Other Forces. *Journal of the Atmospheric Sciences*, **44**, 828-841.

Haynes, P. H., and M. E. McIntyre, 1990: On the Conservation and Impermeability Theorems for Potential Vorticity. *Journal of the Atmospheric Sciences*, **47**, 2021-2031.

Hoskins, B. J., 1991: Towards a PV-Theta View of the General-Circulation. *Tellus Series a-Dynamic Meteorology and Oceanography*, **43**, 27-35.

Hsu, H. H., and X. Liu, 2003: Relationship between the Tibetan Plateau Heating and East Asian Summer Monsoon Rainfall. *Geophysical Research Letters*, **30**, 4.

Huang, J. P., W. Chen, Z. P. Wen, G. J. Zhang, Z. X. Li, Z. Y. Zuo, and Q. Y. Zhao, 2019: Review of Chinese Atmospheric Science Research over the Past 70 Years: Climate and Climate Change. *Science China-Earth Sciences*, **62**, 1514-1550.

Huang, R. H., J. L. Chen, and G. Huang, 2007: Characteristic's and Variations of the East Asian Monsoon System and Its Impacts on Climate Disasters in China. *Advances in Atmospheric Sciences*, **24**, 993-1023.

Jiang, D. B., Z. L. Ding, H. Drange, and Y. Q. Gao, 2008: Sensitivity of East Asian Climate to the Progressive Uplift and Expansion of the Tibetan Plateau under the Mid-Pliocene Boundary Conditions. *Advances in Atmospheric Sciences*, **25**, 709-722.

Kitoh, A., 2004: Effects of Mountain Uplift on East Asian Summer Climate Investigated by a Coupled Atmosphere-Ocean Gcm. *Journal of Climate*, **17**, 783-802.

Kripalani, R. H., and A. Kulkarni, 1997: Climatic Impact of El Niño/La Niña on the Indian Monsoon: A New Perspective. *Weather*, **52**, 39-46.

Kripalani, R. H., and A. Kulkarni, 2001: Monsoon Rainfall Variations and Teleconnections over South and East Asia. *International Journal of Climatology*, **21**, 603-616.

Kubota, H., Y. Kosaka, and S. P. Xie, 2016: A 117-Year Long Index of the Pacific-Japan Pattern with Application to Interdecadal Variability. *International Journal of Climatology*, **36**, 1575-1589.

Liang, X. Y., Y. M. Liu, and G. X. Wu, 2005: Effect of Tibetan Plateau on the Site of Onset and Intensity of the Asian Summer Monsoon. *Acta Meteorologica Sinica*, **63**, 799-805.

Liebmann, B., and C. A. Smith, 1996: Description of a Complete (Interpolated) Outgoing Longwave Radiation Dataset. *Bulletin of the American Meteorological Society*, **77**, 1275-1277.

Liu, X. D., 1999: Influences of Qinghai-Xizang (Tibet) Plateau Uplift on the Atmospheric Circulation, Global Climate and Environment Changes. *Plateau Meteorology*, **18**, 321-332.

Liu, X. D., and Z. Y. Yin, 2002: Sensitivity of East Asian Monsoon Climate to the Uplift of the Tibetan Plateau. *Palaeogeography Palaeoclimatology Palaeoecology*, **183**, 223-245.

Liu, Y. M., M. M. Lu, H. J. Yang, A. M. Duan, B. He, S. Yang, and G. X. Wu, 2020: Land-Atmosphere-Ocean Coupling Associated with the Tibetan Plateau and Its Climate Impacts. *National Science Review*, **7**, 534-552.

Lucchesi, R., 2012: File Specification for Merra Products. Gmao Office Note No. 1 (Version 2.3), 87 pp. [Available at

Https://Gmao.Gsfc.Nasa.Gov/Pubs/Docs/Lucchesi528.Pdf. Accessed on 18 April 2019.]

Ma, T. T., G. X. Wu, Y. M. Liu, Z. H. Jiang, and J. H. Yu, 2019: Impact of Surface Potential Vorticity Density Forcing over the Tibetan Plateau on the South China Extreme Precipitation in January 2008. Part I: Data Analysis. *Journal of Meteorological Research*, **33**, 400-415.

Mitchell, T. D., and P. D. Jones, 2005: An Improved Method of Constructing a Database of Monthly Climate Observations and Associated High-Resolution Grids. *International Journal of Climatology*, **25**, 693-712.

Rienecker, M. M., and Coauthors, 2011: Merra: Nasa's Modern-Era Retrospective Analysis for Research and Applications. *Journal of Climate*, **24**, 3624-3648.

Rossby, C. G., 1940: Planetary Flow Patterns in the Atmosphere. *Quarterly Journal of the Royal Meteorological Society*, **66**, 68-87.

Ryoo, J. M., Y. Kaspi, D. W. Waugh, G. N. Kiladis, D. E. Waliser, E. J. Fetzer, and J. Kim, 2013: Impact of Rossby Wave Breaking on U.S. West Coast Winter Precipitation During Enso Events. *Journal of Climate*, **26**, 6360-6382.

Sandhya, M., S. Sridharan, M. I. Devi, and H. Gadhavi, 2015: Tropical Upper Tropospheric Ozone Enhancements Due to Potential Vorticity Intrusions over Indian Sector. *Journal of Atmospheric and Solar-Terrestrial Physics*, **132**, 147-152.

Sheng, C., and Coauthors, 2021: Characteristics of the Potential Vorticity and Its Budget in the Surface Layer over the Tibetan Plateau. *International Journal of Climatology*, **41**, 439-455.

Wang, B., and Q. Zhang, 2002: Pacific-East Asian Teleconnection. Part Ii: How the Philippine Sea Anomalous Anticyclone Is Established During El Nino Development. *Journal of Climate*, **15**, 3252-3265.

Wang, B., R. Wu, and K. M. Lau, 2001: Interannual Variability of the Asian Summer Monsoon: Contrasts between the Indian and the Western North Pacific-East Asian Monsoons. *Journal of Climate*, **14**, 4073-4090.

Watanabe, M., and M. Kimoto, 2000: Atmosphere-Ocean Thermal Coupling in the North Atlantic: A Positive Feedback. *Quarterly Journal of the Royal Meteorological Society*, **126**, 3343-3369.

Watanabe, M., and F. F. Jin, 2003: A Moist Linear Baroclinic Model: Coupled Dynamical-Convective Response to El Nino. *Journal of Climate*, **16**, 1121-1139.

Watanabe, M., M. Kimoto, T. Nitta, and M. Kachi, 1999: A Comparison of Decadal Climate Oscillations in the North Atlantic Detected in Observations and a Coupled Gcm. *Journal of Climate*, **12**, 2920-2940.

Wei, W., R. H. Zhang, M. Wen, X. Y. Rong, and T. Li, 2014: Impact of Indian Summer Monsoon on the South Asian High and Its Influence on Summer Rainfall over China. *Climate Dynamics*, **43**, 1257-1269.

Wen, N., Z. Liu, and L. Li, 2019: Direct Enso Impact on East Asian Summer Precipitation in the Developing Summer. *Climate Dynamics*, **52**, 6799-6815.

Wu, G. X., Y. P. Cai, and X. J. Tang, 1995: Moist potential vorticity and slantwise vorticity development (in Chinese). *Acta Meteorologica Sinica*, **53**, 387-405.

Wu, G. X., and Y. P. Cai, 1997: Vertical wind shear and down-sliding slantwise vorticity development (in Chinese). *Chinese Journal of Atmospheric Sciences*, **21**, 273-282.

Wu, G., Y. Liu, B. Dong, X. Liang, A. Duan, Q. Bao, and J. Yu, 2012: Revisiting Asian Monsoon Formation and Change Associated with Tibetan Plateau Forcing: I. Formation. *Climate Dynamics*, **39**, 1169-1181.

Wu, G. X., and Y. S. Zhang, 1998: Tibetan Plateau Forcing and the Timing of the Monsoon Onset over South Asia and the South China Sea. *Monthly Weather Review*, **126**, 913-927.

Wu, G. X., W. J. Li, and H. Guo, 1997: Sensible Heat Driven Air-Pump over the Tibetan Plateau and Its Impacts on the Asian Summer Monsoon. In: Ye Dz (Ed.). Collection in Memory of Zhao Jiuzhang, Science Press, Beijing, 116-126.

Wu, G. X., Y. M. Liu, B. He, Q. Bao, and Z. Q. Wang, 2018: Review of the Impact of the Tibetan Plateau Sensible Heat Driven Air-Pump on the Asian Summer Monsoon. *Chinese Journal of Atmospheric Sciences*, **42**, 488-504.

Wu, G. X., and Coauthors, 2007: The Influence of Mechanical and Thermal Forcing by the Tibetan Plateau on Asian Climate. *Journal of Hydrometeorology*, **8**, 770-789.

Wu, R., 2002: A Mid-Latitude Asian Circulation Pattern in Boreal Summer and Its Connection with the Indian and East Asian Summer Monsoons. *International Journal of Climatology*, **22**, 1879-1895.

Xie, S. P., Y. Kosaka, Y. Du, K. Hu, J. S. Chowdary, and G. Huang, 2016: Indo-Western Pacific Ocean Capacitor and Coherent Climate Anomalies in Post-ENSO Summer: A Review. *Advances in Atmospheric Sciences*, **33**, 411-432.

Xie, S. P., K. M. Hu, J. Hafner, H. Tokinaga, Y. Du, G. Huang, and T. Sampe, 2009: Indian Ocean Capacitor Effect on Indo-Western Pacific Climate During the Summer Following El Niño. *Journal of Climate*, **22**, 730-747.

Xu, X., T. Zhao, X. Shi, and C. Lu, 2015: A Study of the Role of the Tibetan Plateau's Thermal Forcing in Modulating Rainband and Moisture Transport in Eastern China. *Acta Meteorologica Sinica*, **73**, 20-35.

Yanai, M. H., C. F. Li, and Z. S. Song, 1992: Seasonal Heating of the Tibetan Plateau and Its Effects on the Evolution of the Asian Summer Monsoon. *Journal of the Meteorological Society of Japan*, **70**, 319-351.

Yang, J. L., Q. Y. Liu, S. P. Xie, Z. Y. Liu, and L. X. Wu, 2007: Impact of the Indian Ocean Sst Basin Mode on the Asian Summer Monsoon. *Geophysical Research Letters*, **34**, 5.

Ye, D. Z., and Y. X. Gao, 1979: The Meteorology of the Qinghai–Xizang (Tibet) Plateau. *China: Science Press, 278pp*.

Ye, D. Z., S. W. Luo, and B. Z. Zhu, 1957: The Wind Structure and Heat Balance in the Lower Troposphere over Tibetan Plateau and Its Surroundings. *Acta Meteorologica Sinica*, **28**, 108-121.

Yu, J. H., Y. M. Liu, T. T. Ma, and G. X. Wu, 2019: Impact of Surface Potential Vorticity Density Forcing over the Tibetan Plateau on the South China Extreme Precipitation in January 2008. Part Ⅱ: Numerical Simulation. *Journal of Meteorological Research*, **33**, 416-432.

Zhang, G. S., J. Y. Mao, G. X. Wu, and Y. M. Liu, 2021: Impact of Potential Vorticity Anomalies around the Eastern Tibetan Plateau on Quasi-Biweekly Oscillations of Summer Rainfall within and South of the Yangtze Basin in 2016. *Climate Dynamics*, **56**, 813-835.

Zhao, P., and L. X. Chen, 2001: Climate Features of Atmospheric Heat Source/Sink over the Qinghai-Xizang Plateau in 35 Years and Its Relation to Rainfall in China. *Science in China Series D-Earth Sciences*, **44D**, 858-864.

Zhao, L. and Y. H. Ding, 2009: Potential vorticity analysis of cold air activities during the East Asian summer monsoon (in Chinese). *Chinese Journal of the Atmospheric Sciences*, **33**, 359-374.

Zhou, X. Y., F. Liu, B. Wang, B. Q. Xiang, C. Xing, and H. Wang, 2019: Different Responses of East Asian Summer Rainfall to El Nino Decays. *Climate Dynamics*, **53**, 1497-1515.

Zuo, Z. Y., R. H. Zhang, and P. Zhao, 2011: The Relation of Vegetation over the Tibetan Plateau to Rainfall in China During the Boreal Summer. *Climate Dynamics*, **36**, 1207-1219.

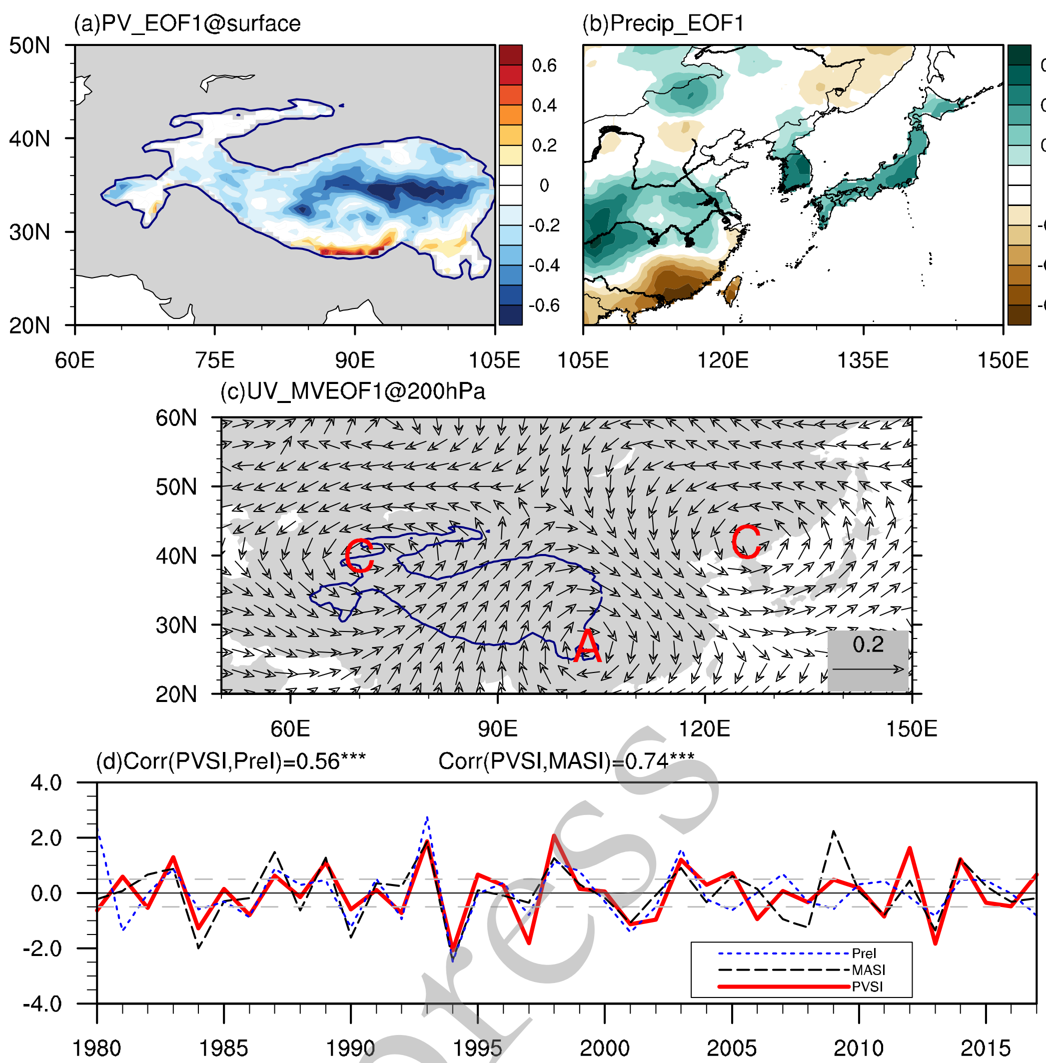

Fig. 1. Spatial distribution of the first leading mode of variation in boreal summer for (a) surface PV over the TP; (b) precipitation over East Asia; and (c) circulation over East Asia at 200 hPa. (d) Corresponding normalized principal components of the first EOF mode are shown in (a), (b) and (c). The blue line in (a, c) denotes the TP topographic boundary of 3,000 m.

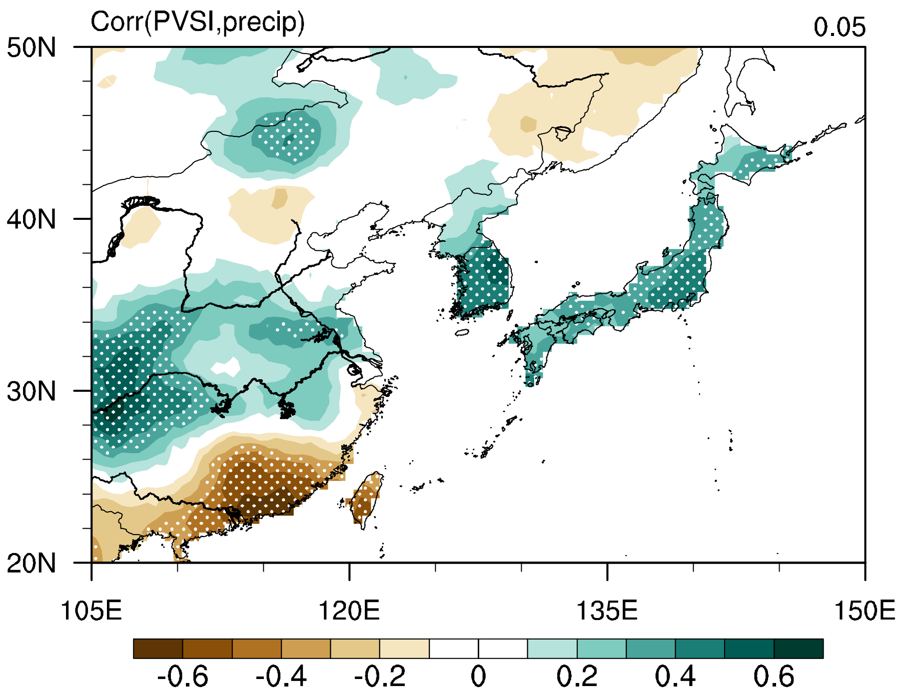

Fig. 2. Spatial distribution of the correlation coefficients between the PVSI and rainfall anomalies downstream. Areas exceeding the 0.05 significance level are highlighted with dots.

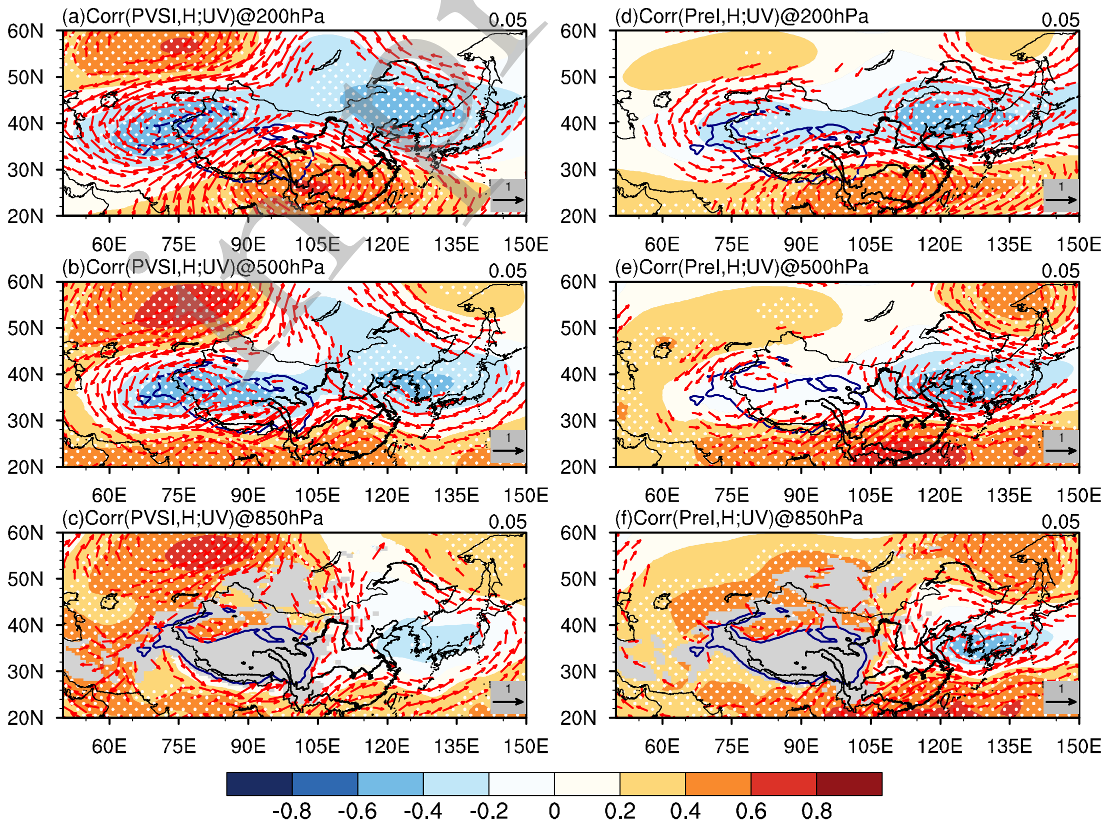

Fig. 3. Spatial distribution of the correlation coefficient between the PVSI and geopotential height anomalies (shading) and circulation anomalies (vector, those passing the 0.05 significance level are shown) at (a) 200 hPa; (b) 500 hPa; and (c) 850 hPa. Figures (d-f) are the same as Figures (a-c), but for PreI. Areas exceeding the 0.05 significance level are highlighted with dots. The blue line denotes the TP topographic boundary of 3,000 m.

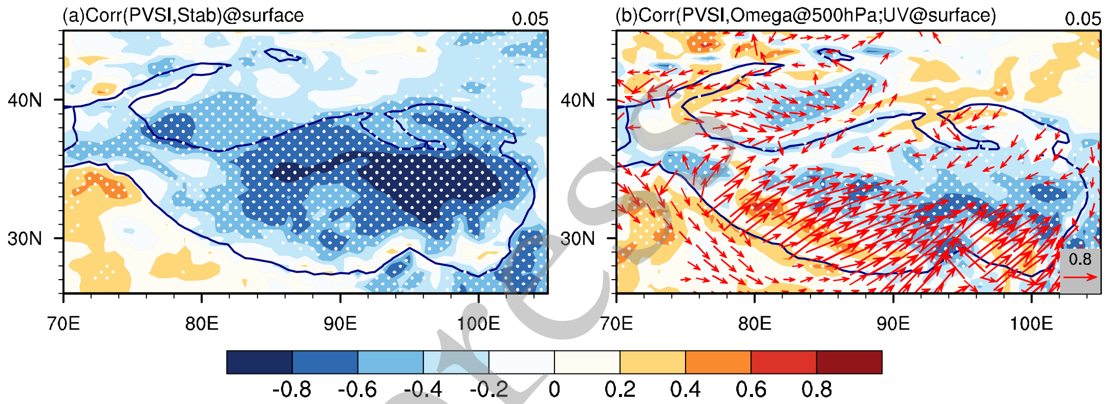

Fig. 4. Spatial distribution of the correlation coefficient between the PVSI and (a) surface static stability anomalies and (b) horizontal wind anomalies at the surface (vector, those exceeding the 0.05 significance test are shown) and omega at 500 hPa (shading). Areas exceeding the 0.05 significance level are highlighted with dots. The blue line denotes the TP topographic boundary of 3,000 m.

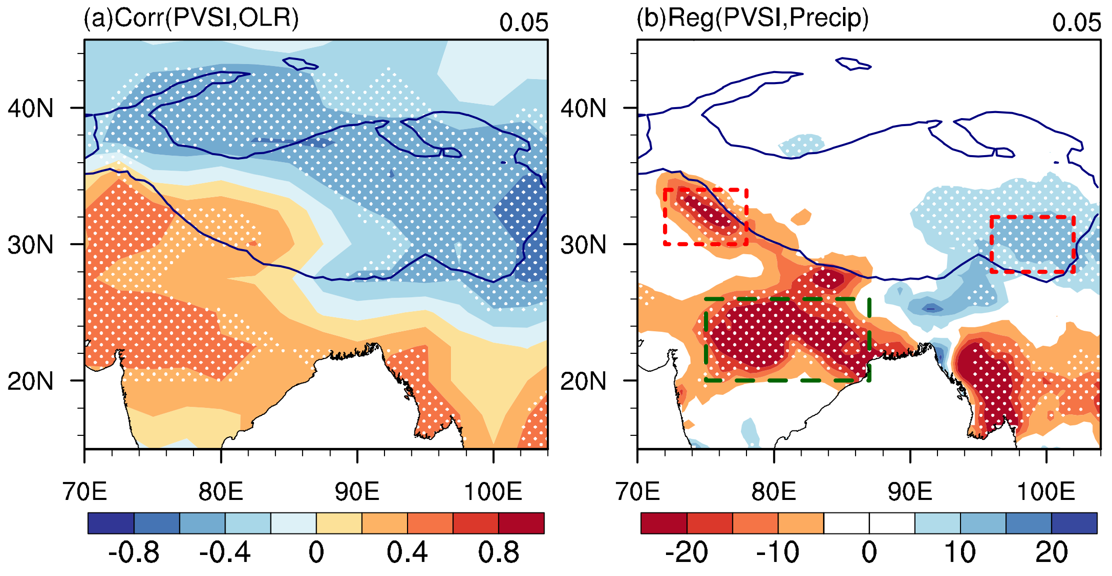

Fig. 5. Spatial distribution of the (a) correlation coefficient between the PVSI and OLR anomalies and (b) regressed rainfall anomalies against the PVSI (units: mm/month). Areas exceeding the 0.05 significance level are highlighted with dots. The blue line denotes the TP topographic boundary of 3,000 m.

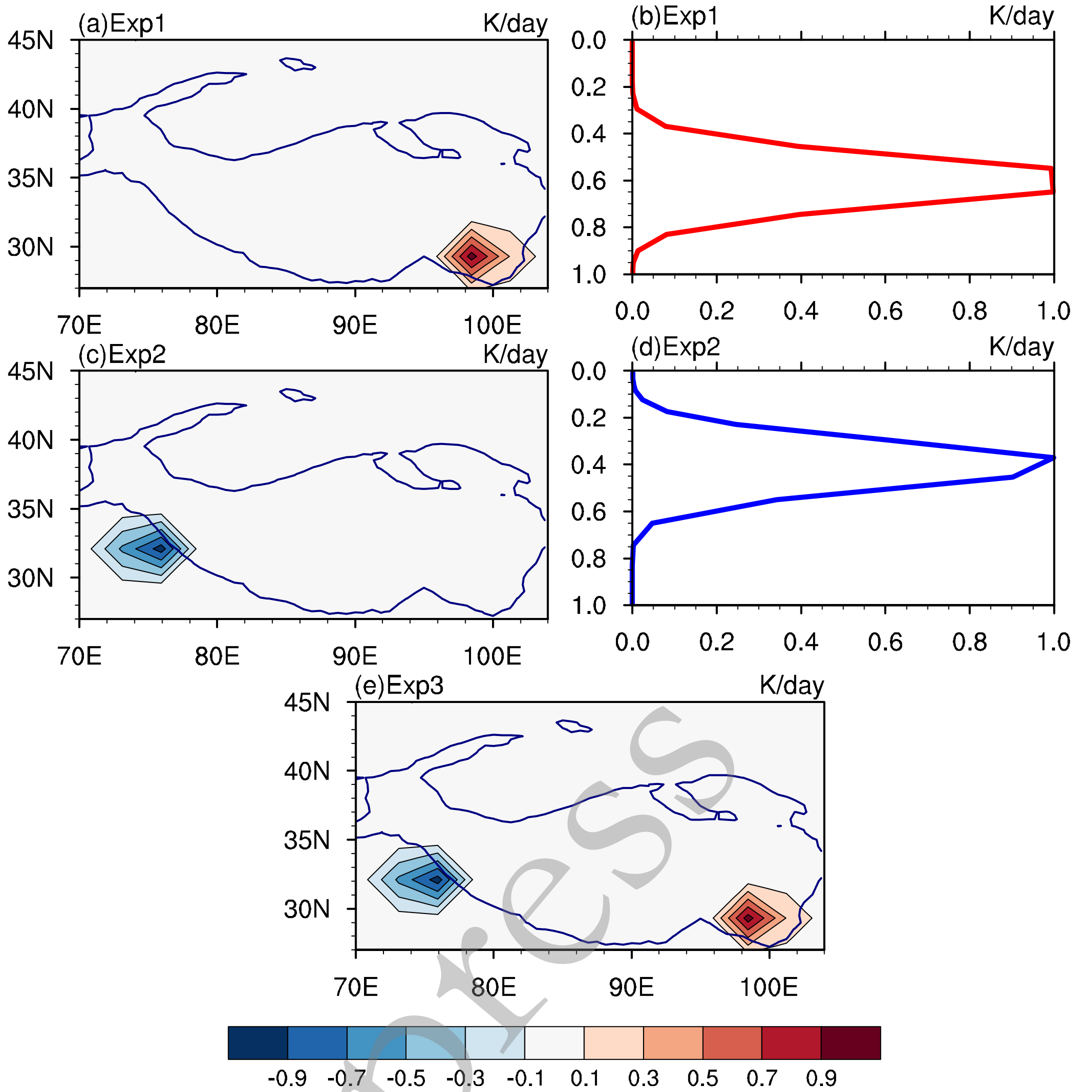

Fig. 6. Specified ideal diabatic heating (units: K/day) horizontal distribution in (a) Exp1; (c) Exp2; and (c) Exp3. Specified ideal diabatic heating (units: K/day) profiles in (b) Exp1 and (d) Exp2. The blue line denotes the TP topographic boundary of 3,000 m.

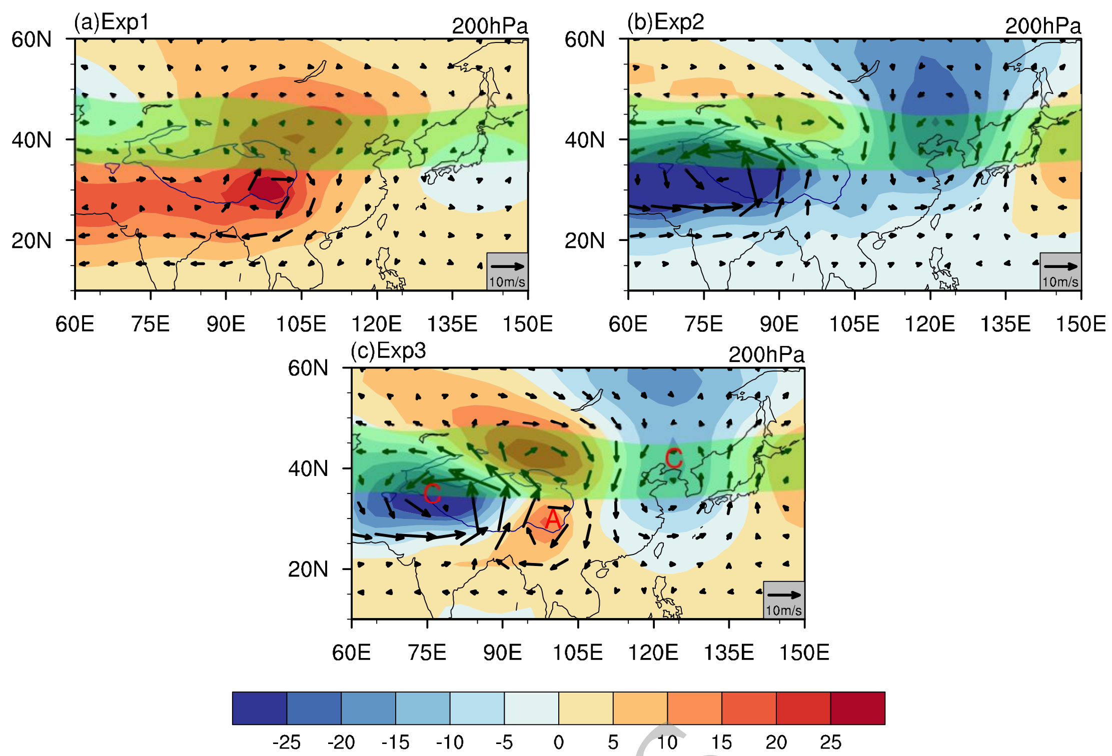

Fig. 7. Responses of geopotential height (shading, units: gpm) and horizontal wind (vector, units: m/s) at 200 hPa in (a) Exp1; (b) Exp2; and (c) Exp3. The blue line denotes the TP topographic boundary of 3,000 m. The light green shading indicates a westerly jet with a zonal wind speed greater than 20 m/s at 200 hPa.

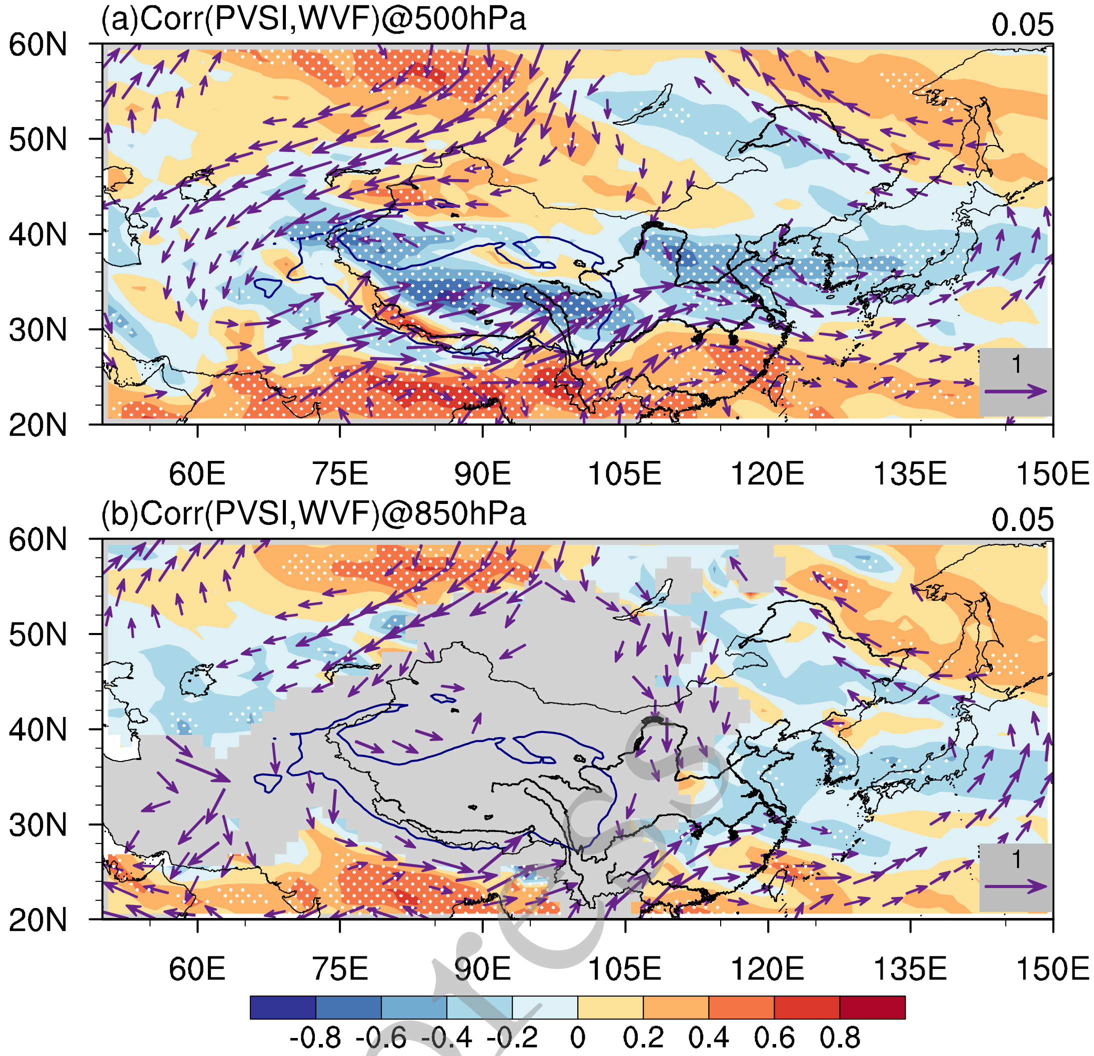

Fig. 8. Spatial distribution of the correlation coefficient between the PVSI and the divergence of WVF anomalies (shading) and WVF anomalies (vector, those passing the 0.05 significance level are shown) at (a) 500 hPa and (b) 850 hPa. Areas exceeding the 0.05 significance level are highlighted with dots. The blue line denotes the TP topographic boundary of 3,000 m.

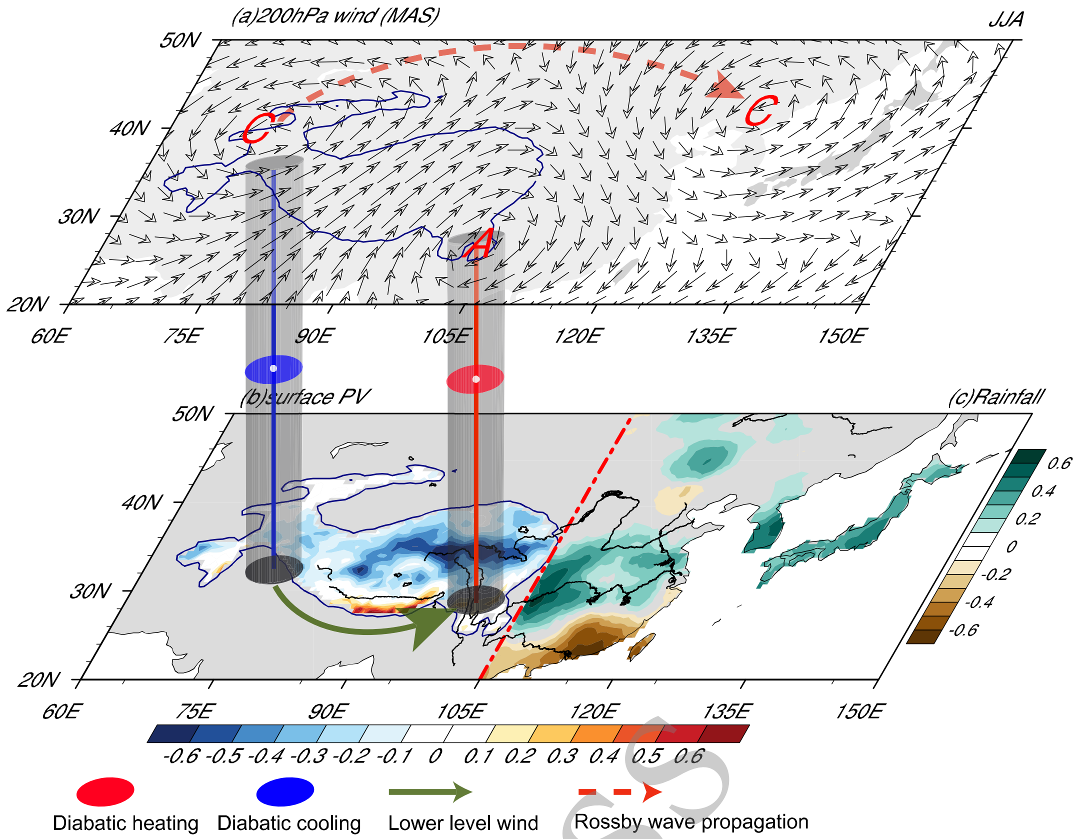

Fig. 9 Schematic showing the interannual surface TPPV influence on EASR. (a) Anomalous 200 hPa wind associated with surface TPPV forcing; (b) anomalous surface TPPV; and (c) same as (a) but for rainfall anomalies. The red (blue) circle indicates diabatic heating (cooling). The green (red) vector indicates the lower-level wind (upper-level Rossby wave propagation).